Review

Scaling of maximum net force output by motors used for locomotion

James H. Marden

208 Mueller Laboratory, Department of Biology, University Park, PA 16802, USA

e-mail: jhm10@psu.edu

Summary

Biological and engineered motors are surprisingly similar in their adherence to two or possibly three fundamental regimes for the mass scaling of maximum force output (F_{max}). One scaling regime (Group 1: myosin, kinesin, dynein and RNA polymerase molecules; muscle cells; whole muscles; winches; linear actuators) comprises motors that create slow translational motion with force outputs limited by the axial stress capacity of the motor, which results in F_{max} scaling as motor mass$^{0.67}$ ($M^{0.67}$). Another scaling regime (Group 2: flying birds, bats and insects; swimming fish; running animals; piston engines; electric motors; jets) comprises motors that cycle rapidly, with significant internal and external accelerations, and for whom inertia and fatigue life appear to be important constraints. The scaling of inertial loads and fatigue life both appear to enforce F_{max} scaling as $M^{1.0}$ in these motors. Despite great differences in materials and mechanisms, the mass specific F_{max} of Group 2 motors clusters tightly around a mean of 57 N kg^{-1}, a region of specific force loading where there appears to be a common transition from high- to low-cycle fatigue. For motors subject to multi-axial stresses, the steepness of the load–life curve in the neighborhood of 50–100 N kg^{-1} may overwhelm other material and mechanistic factors, thereby homogenizing the mass specific F_{max} of grossly dissimilar animals and machines. Rockets scale with Group 1 motors but for different mechanistic reasons; they are free from fatigue constraints and their thrust is determined by mass flow rates that depend on cross sectional area of the exit nozzle. There is possibly a third scaling regime of F_{max} for small motors (bacterial and spermatazoan flagella; a protozoan spring) where viscosity dominates over inertia. Data for force output of viscous regime motors are scarce, but the few data available suggest a gradually increasing scaling slope that converges with the Group 2 scaling relationship at a Reynolds number of about 10^2. The Group 1 and Group 2 scaling relationships intersect at a motor mass of 4400 kg, which restricts the force output and design of Group 2 motors greater than this mass. Above 4400 kg, all motors are limited by stress and have F_{max} that scales as $M^{0.67}$; this results in a gradual decline in mass specific F_{max} at motor mass greater than 4400 kg. Because of declining mass specific F_{max}, there is little or no potential for biological or engineered motors or rockets larger than those already in use.

Introduction

Movement is a pervasive feature of microbial and animal biology, from bacteria moving over tiny distances to whales migrating across hemispheres. This broad range of size, mechanisms and ecology makes locomotion an attractive topic for scaling studies (recent examples include Iriate-Diaz, 2002; McHenry and Jed, 2003). Machines built by humans to create motion also vary broadly in size and usage, and interest in micro- and nanoscale machines (Ellington, 1999) is bringing engineered motors into a size range more traditionally the realm of biology. Interestingly, there are unanticipated convergences in certain performance characteristics of all types of motors (Fig. 1; Marden and Allen, 2002), which suggests that biologists and engineers have much to share in terms of data, analyses and insights.

To move, a body must produce a net directional force on its surroundings. The resulting acceleration, equal to the ratio of force to mass, is broadly relevant for biological events whose outcome is determined by how well an organism can change its speed (Marden, 1989; Wickman, 1992; Bowlin and Winkler, 2004) or resist an external acceleration such as gravity. Hence, examination of net force production in relation to mass is one possible starting point for understanding scale effects in locomotion. Here I present a short review of what is known about the mass scaling of
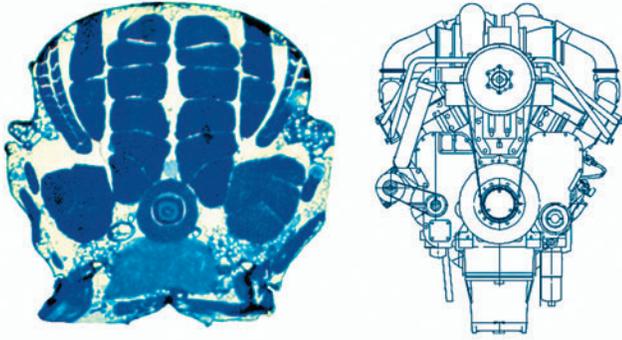
Fig. 1. Cross section of a *Drosophila melanogaster* (fruit fly) thorax (ca. 0.0003 g) and a diesel engine (118 681 kg). Along with superficial shape similarities, vastly different motors have very similar performance in terms of force output per motor mass. (*Drosophila* image courtesy of R. Ordway.)

propulsive forces generated by both animate and inanimate motors.

Motors and data included in this study

Data for this paper come primarily from a recent study of the scaling of net force output as a function of motor mass for a wide array of biological and engineered motors (Marden and Allen, 2002; see that paper for data sources). Briefly, the data set comprises the force output and motor mass of single molecules (myosin, kinesin, dynein, RNA polymerase); molecular motors (F_0–F_1 ATPase ion pump, *Escherichia coli* flagella, mammalian sperm and the spasmoneme spring of the protozoan *Vorticella*); muscle cells; whole muscles; flying insects, birds and bats; swimming crayfish and fish; running cockroaches, iguanas, kangaroo rats, dogs and humans; jet engines; piston engines; rockets; linear electric motors (including an artificial human heart); rotary electric motors; winches and hoists; linear actuators; and materials testing machines.

For each of these motors we were able to find data or specifications reporting maximum force output and motor mass. Force outputs are the net force vector that can be maintained in a steady fashion, although not necessarily indefinitely. Importantly, these data do not include instantaneous peak forces. For example, data for running animals comprise the time averaged net force vector from force plate recordings obtained by integrating over one complete stride cycle (including the interval between ground contact phases). Force output of flying animals was determined from maximum load lifting (i.e. an average over many complete wingbeat cycles), whereas for swimming animals it was calculated from body acceleration during fast starts that also comprise several stroke cycles. Force outputs of machines are the maximum steady-state thrust or pulling force. For machines typically used to generate torque, the radius of the crankshaft (piston engines) or the shaft that exits the motor (rotary electrical motors) was factored out to derive net force output. Because these measures all represent cycle-averaged net force

output, they are directly comparable. This makes it possible to compare data from a wide array of biological and engineered devices.

Mass of engineered motors is the mass of the motor with no attached machinery and does not include the mass of fuel. The one exception is rockets, which consume their mass in order to generate force; we therefore included fuel in the estimates of rocket mass. In a few cases where motor mass was not reported, we were able to estimate motor mass based on dimensional data and density (molecular motors) or on approximate ratios of limb to total body mass (running animals). Mass of animal motors is the total mass of the muscles and limbs that created the net force measured during flying or running. For swimming animals, published data for motor mass include only total mass of the muscles involved in swimming. It would be preferable to include the additional mass of skeletal components of the swimming motor, but those components are probably less then 10% of motor mass and their omission has no meaningful impact on the results.

It is not a simple task to define precisely what constitutes a motor, so to compile a broad and inclusive data set we adopted a hierarchical approach. Included in the data are examples of minimally functional motor units with no external levers (molecules; individual muscles with no attached limbs; electric and piston motors with no attached external gears or levers; jets; rockets) along with devices in which lever systems are closely integrated with the motive components (animal limb systems; winches and hoists; electric motors with attached gear boxes). In certain cases we treat separately data for different hierarchical levels of a single motor. Such examples include single muscles *versus* the whole limb systems in which they operate, and electric winch motors *versus* whole winches.

Scaling of motor force output: fundamental scaling regimes

These compiled data reveal two fundamental scaling regimes for motor force output, and there may be a third scaling regime for very small motors operating in the viscous regime for which there are presently only scant data. These regimes are described in the following paragraphs.

Group 1: translational motors whose maximum force output scales as motor mass$^{0.67}$

Motors that push or a pull a load in steady translational (i.e. linear) motion have force outputs that scale as the two-thirds power of motor mass (Fig. 2). This group of motors comprises single molecules (myosin, kinesin, dynein and RNA polymerase), muscle cells, whole muscles, winches, linear actuators and rockets.

Group 2: motors whose maximum force output scales as motor mass$^{1.0}$

At sizes where inertial forces dominate (fruit fly size and above), motors that cycle at a steady rate and are used to move bodies in a fashion more complex than translation have

maximal force outputs that scale as motor $M^{1.0}$ (Fig. 3), with motor mass-specific net force output averaging a relatively
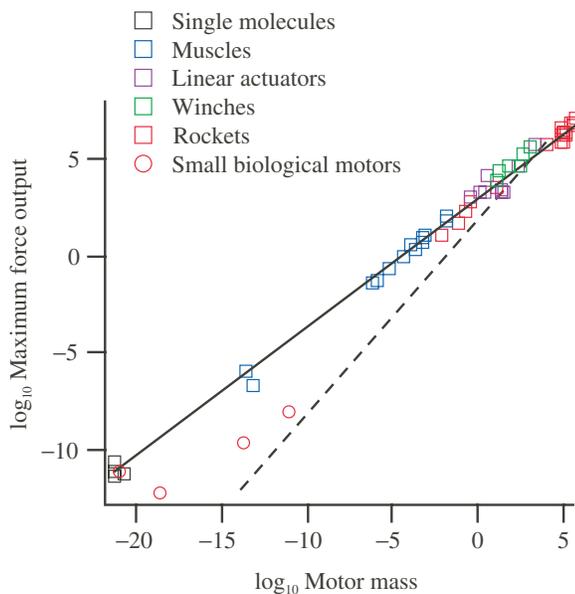

Fig. 2. Maximum force output by translational motion motors (Group 1) as a function of their mass. The least squares fit (solid line) is: $F_{max}=891\ M^{0.67}$. The dashed line is the scaling fit for Group 2 motors in which F_{max} scales as $M^{1.0}$ (Fig. 3). Maximum force output (N) and motor mass (kg).
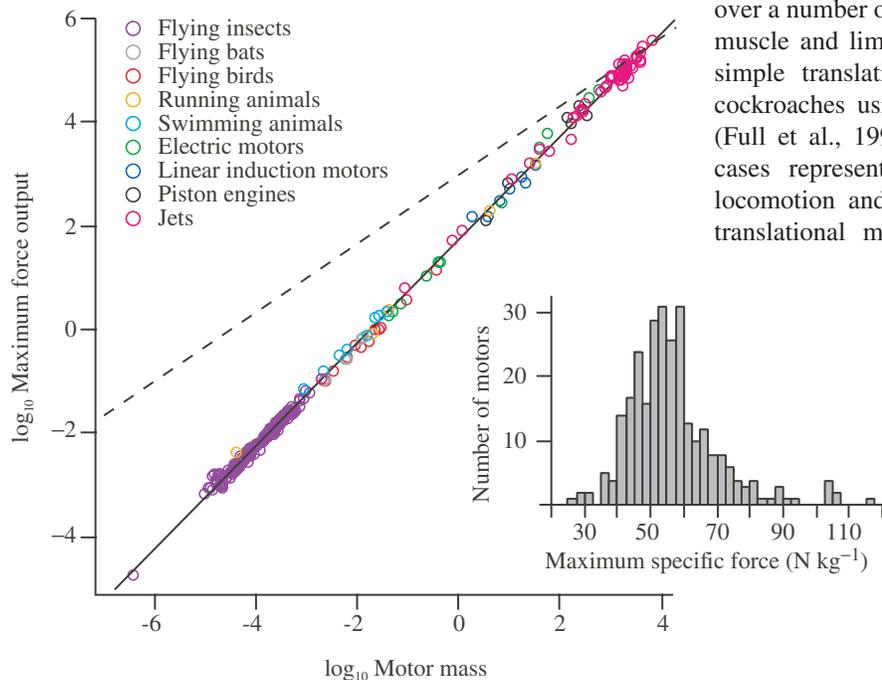

Fig. 3. Maximum force output by Group 2 motors as a function of their mass. The least squares fit (solid line) is: $F_{max}=55\ M^{0.999}$. The dashed line is the scaling fit for Group 1 motors for which F_{max} scales as $M^{0.67}$ (Fig. 2). Inset: the frequency distribution of mass specific force output for all of the Group 2 motors on the main plot. Maximum force output (N) and motor mass (kg).

invariant 57 N kg^{-1} (Fig. 3 inset; standard deviation= 14 N kg^{-1}). This set of motors includes the locomotor apparatus of flying birds, bats and insects, swimming fish, running animals, piston engines, electric motors and all types of jets.

Table 1 shows the scaling relationships within each of the general types of Group 1 and Group 2 motors. Notably, both the slopes and the intercepts tend to be quite similar to the group means, i.e. the scaling regimes apply equally well for motor types within groups.

Robustness of the data: comparisons with divergent predictions

Maximal force outputs of the Group 2 motors shown in Fig. 3 are clustered tightly around a single universal scaling relationship. This is surprising considering the diversity of materials and mechanisms and the widely different methods used to determine F_{max}. Equally surprising is that this universality of specific force output escaped the notice of both biologists and engineers until very recently (Marden and Allen, 2002). Thus, it is reasonable and appropriate to question the validity of the result. I am asked frequently if we either consciously or unconsciously filtered the data, excluding points that did not fit the relationship and thereby to some extent manufacturing the tight fit.

Our approach was to include all instances for which we could find motor mass and a measure of maximal net force output for a defined mechanical situation that measured a force output vector that was either steadily maintained or averaged over a number of cycles. We omitted biological data for which muscle and limb systems were used in a fashion other than simple translation, but not steady cycling. Examples are cockroaches using their limbs to push against fixed objects (Full et al., 1995) and human weight-lifting records. These cases represent neither simple translation or multi-cycle locomotion and the force outputs should be close to what translational motors produce when attached to the lever systems of animal limbs (i.e. a reduction in translational force caused by levers that amplify speed and distance). We also omitted data for devices such as stepper motors, whose specific force outputs resemble translational motors at slow step rates, but approach the specific force outputs of Group 2 motors when used at high step rates. In general, there are potentially many force outputs by translational motors used at intermediate speeds or attached to force-reducing lever systems (e.g. biting forces produced by an animal jaw; Alexander, 1985) that fall between the two fundamental scaling relationships represented by our sample in Groups 1 and 2.

Two recent research efforts provide particularly good tests of the robustness

Table 1. *Fitting terms from least squares linear regressions of $\log_{10}$ Maximum force output (N) as a function of $\log_{10}$ Motor mass (kg) for different types of motors*

Motor type	Intercept	Slope	r^2	N	S.E.M. slope	Min mass	Max mass
Group 1							
Muscles	2.995	0.677	0.997	16	0.010	4.8×10^{-22}	0.014
Rockets	2.737	0.719	0.988	19	0.019	0.0079	5.87×10^5
Winches	3.251	0.736	0.852	6	0.154	14.5	1361
Linear actuators	3.048	0.612	0.656	9	0.167	0.34	2587
Mean	3.008	0.686					
Group 2							
Running animals	1.703	0.949	0.998	5	0.023	0.00004	32.7
Swimming animals	1.672	0.924	0.992	8	0.033	0.0009	0.04
Flying birds	1.555	0.959	0.993	11	0.026	0.002	0.37
Flying bats	1.862	1.082	0.994	7	0.037	0.002	0.013
Flying insects	1.583	0.959	0.982	149	0.011	3.7×10^{-7}	0.008
Turbines	1.811	0.963	0.993	21	0.018	0.002	4264
Turbofans	1.793	0.986	0.934	30	0.049	64	6804
Electric rotary motors	1.739	1.078	0.999	10	0.013	0.04	558
Linear induction motors	1.825	0.854	0.940	7	0.096	1.9	32.6
Piston engines	1.719	1.016	0.988	31	0.021	0.165	2744
Mean	1.726	0.977					

N shows the sample size within each category of motor; S.E.M. is the standard error of the least squares regression slope. Minimum and maximum motor masses (kg) are shown for each category. Single molecules that create translational motion (myosin, kinesin, dynein, RNA polymerase) are included here with muscle cells and whole muscles (treating muscles alone yields a nearly identical scaling equation). Piston engines greater than 4400 kg mass are excluded because they scale differently than smaller piston engines (see text and Fig. 10).

of the tight scaling fit for Group 2 motors, for in both instances the authors hypothesized a different result. In the first case, Dudley (2002) questioned the suitability of the load-lifting technique that was used to obtain force outputs of flying animals and stated that the scaling of force production for flying animals is unresolved. Subsequently, Dillon and Dudley (2004) used a different method to obtain the scaling of maximal force output of flying euglossine bees, but they did not compare their results with previous data. Here I have converted their load lifting data into units of vertical force (N) and motor mass (kg) and compare them (Fig. 4) with all of the insect load lifting data from previous scaling studies (Marden, 1987; Marden and Allen, 2002). The two sets of data are indistinguishable.

A second interesting case is that of the MIT Microjet, a tiny turbine motor (0.002 kg mass) built from silicon wafers (Epstein et al., 2000). In the planning and early fabrication phases of this completely novel design, the microjet was predicted to produce a thrust-to-weight ratio of about 100:1 (Epstein and Senturia, 1997), which is 1000 N kg^{-1} thrust-to-mass. This hypothesis was based on the assumption that force output for all types of devices should scale with cross-sectional area, which would radically increase the ratio of thrust to mass for very small motors. Despite the goal and prediction of a very high specific thrust, the finished microjet produced a maximum thrust-to-mass of 55 N kg^{-1} (Fig. 4), which is almost exactly the average value of Dillon and Dudley's bees (57 N kg^{-1}) and the entire set of Group 2 motors shown in Fig. 3 (57 N kg^{-1}).

Group 3: Variable scaling in the transition between viscous and inertial motors

For very small biological motors (N=3) that comprise more than one or a few molecules, force output does not scale as
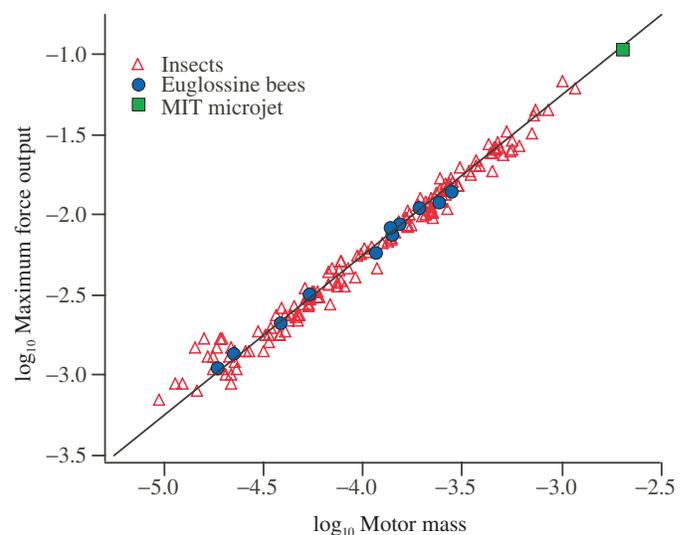

Fig. 4. Maximum force output in relation to motor mass by a selection of Group 2 motors (flying insects; Marden, 1987), along with data from two studies that predicted either vastly different (microjet; Epstein et al., 2000) or subtly different (euglossine bees; Dillon and Dudley, 2004) results. These comparisons demonstrate the robustness of the $M^{1.0}$ scaling and a mean specific force of 57 N kg^{-1} for these types of motors. Maximum force output (N) and motor mass (kg).
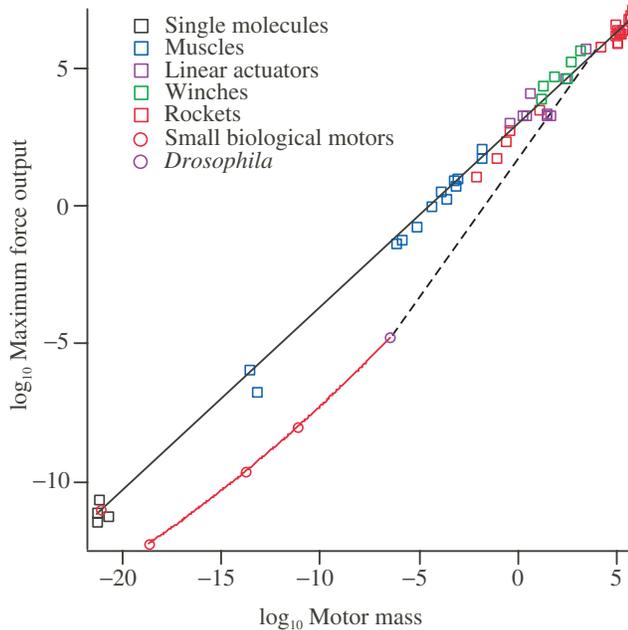
Fig. 5. Force outputs of small Group 3 motors (red curve) that operate in the viscous regime. For comparison, data are included for Group 1 motors, along with a dashed line representing Group 2 motors. The scaling curve for Group 3 motors connects their performance with that of the smallest Group 2 motor (fruit fly). Maximum force output (N) and motor mass (kg).

either $M^{0.67}$ or $M^{1.0}$ as it does in all of the other motors in this survey (Fig. 5). This set of motors includes the *E. coli* flagellar motor, the flagellar motor of mammalian sperm and the helical spring of the protozoan *Vorticella*. These organisms operate over a range of Reynolds numbers in a fluid environment where the main resistive force is viscosity and inertia is much less significant. From Stokes law, the viscous force resisting movement at a given velocity scales according to a linear body dimension. Therefore, the force output would need to scale as approximately $M^{0.33}$ to overcome viscous resistive forces.

Because there are so few data points for this group of viscous regime motors, Marden and Allen (2002) did not treat them separately or estimate a scaling exponent. Throwing such caution to the wind, an original hypothesis is presented here. Reynolds numbers change continuously with increasing size as the ratio of inertial to viscous forces increases. A swimming bacterium operates at Reynolds numbers of about 10^{-6}, compared with 10^{-2} for a swimming sperm (Vogel, 1988). The flight motor of *Drosophila* operates at a Reynolds number of about 10^2 (Dickinson et al., 1999). Over the size range from *E. coli* to *Drosophila*, we can predict that there would not be a single scaling slope that accurately describes force output, since the need to overcome viscous forces gives way gradually to the need to overcome inertial forces. Rather, there should be a gradual increase in the mass scaling exponent of force output over this size range. Despite the very

small sample ($N=4$ when *Drosophila* is included), the data support this hypothesis (Fig. 5), as the four log-log data points can be fit quite precisely by a curve that has a first-order slope of 0.51 and a second-order slope of 0.01. Thus, it appears that the scaling of force output for this group of very small motors falls between $M^{0.33}$ and $M^{1.0}$, with a gradual increase in the scaling slope as viscosity gives way gradually to inertia as the primary force resisting motion. More data in this size range are required before this can be considered a well supported result.

One interesting and very different type of biological motor in this size range that has not yet been examined for force output is the molecular motor of the Apicomplexa, a phylum of primarily unicellular parasites (~5000 species) that includes medically important genera such as *Plasmodium*, *Toxoplasma* and *Cryptosporidium*, along with gregarine parasites that are prevalent in invertebrates. Apicomplexans move by processive movement of F-actin in the plasma membrane. The actin is attached *via* aldolase to a secreted adhesive complex that sticks to the host cell surface (Sibley, 2004). Just inside the plasma membrane are myosin molecules; these typically move the more exteriorly located F-actins in a posterior direction, although directionality is rapidly reversible. This unusual form of actin–myosin interaction allows the parasite to glide at slow speeds while they push past obstacles and penetrate host cells (Dobrowolski and Sibley, 1996; Barragan and Sibley, 2003).

The myosin-coated surface of apicomplexans appears at first glance to be analogous to a muscle turned inside-out. Note however some very important differences in organization that strongly affect function. The apicomplexan actomyosin motor is only a small layer of molecules around the cell periphery rather than throughout the cross section as occurs in muscle, so force output should scale with body circumference (i.e. $M^{0.33}$; this matches the scaling of resistive forces in the viscous regime). In addition, they have no lengthwise sarcomeric organization, which in muscles allows units in a linear series to shorten simultaneously and attain whole-muscle shortening speeds that are an approximately constant number of muscle lengths per time (i.e. muscle contractile speed scales as L^1). Lacking any contractile ability or appendages, apicomplexans can move only at the processive speed of single myosin molecules, regardless of the number of myosins acting in series (i.e. speed scales as L^0). As a result of these design factors, the larger apicomplexans are very slow for their size. Small apicomplexans have been reported to move at speeds of 1–10 $\mu m\ s^{-1}$ (Sibley, 2004) and I have filmed large gregarines of 0.3 mm length gliding on glass microscope slides at speeds up to 20 $\mu m\ s^{-1}$, less than 10^{-1} body lengths per second. This pales in comparison with the roughly 10^2 body lengths per second flight speed of the dragonflies that carry these gregarines. This example nicely demonstrates that sarcomeres, by virtue of their volume-filling design and in-series connection of contractile units, have evolved to increase greatly both the speed and the force of locomotion.

Hypotheses to explain these scaling regimes

An ultimate stress hypothesis for $M^{0.67}$ *scaling of Group 1 motors*

Except for rockets (discussed separately below), the maximum force outputs of Group 1 motors occur at conditions where external motion has stopped (i.e. the motor force output equals the resistive force of the load) and there is no internal or external acceleration or mechanical power output. The maximum force that can be generated by a motor designed to generate large external forces at low or zero velocity is limited by the failure point of the most critical element (i.e. the weakest link). Optimal design in this context occurs when all component parts are equally near their critical yielding or breaking stress, no link is consistently the weakest and all parts should fail nearly simultaneously (*sensu* Mattheck, 1998; otherwise certain parts are either unnecessarily bulky or excessively weak). Hence, for an optimally designed motor of this type, we would expect that maximum force is close to mechanical failure force, which for uniaxial stress occurs across a critical plane (Norton, 2000). Load capacity should therefore scale as approximately the cross sectional area of the motor, or $M^{0.67}$.

Maximum force generated by individual molecules such as myosin occurs just prior to breakage of the molecular linkage with the substrate (Finer et al., 1994); muscles and tendons frequently tear during heavy exertion (Orchard, 2002); and the maximal forces reported here for linear actuators and winches is at or near the static force levels that cause mechanical breakage. Thus, it appears that stress limitations are the primary mechanism underlying the $M^{0.67}$ scaling of maximal force output by translational motors. This hypothesis explains the scaling slope for F_{max} for all of the Group 1 motors, but it does not explain why the data can be described by a single regression line rather than a family of parallel lines. Note however that there is significant scatter around the line (an approximate 10-fold range of variation at any given motor mass) that presumably reflects differences in material properties and mechanisms that affect stress resistance.

A fatigue-life hypothesis for $M^{1.0}$ *scaling and the tight clustering of maximum specific force outputs of Group 2 motors around 57 N kg^{-1}*

What explains the remarkably tight clustering (Figs 3, 4) of maximum specific force output around a single $M^{1.0}$ scaling relationship for things as different as animals, piston engines, electric motors and jets? The following paragraphs present a novel hypothesis based on fatigue resistance and general scaling principles to explain this surprising convergence of motor performance.

Group 2 motors do not fail in the same way as do translational motors. Rather than critical stress, failure in Group 2 motors occurs primarily by factors such as overheating, creep and either low- or high-cycle fatigue (Norton, 2000), all of which are time-dependent (number of cycles at a given load) and are exacerbated by complex multiaxial stresses (pushes and pulls in a variety of directions and phases) of the kind experienced by motors such as animal limbs (Blob and Biewener, 2001), cycling pistons and high-speed rotating turbines (Mattingly, 2002).

Materials science analyses that examine the relationship between multiaxial stress and lifespan are gradually becoming more common and sophisticated (Fischer et al., 1998; Sonsino, 2001; Niebur et al., 2002), but there is not yet an empirical or theoretical understanding that specific load affects durability in a common fashion across many different types of materials and devices. I suggest that there is such a relationship and here I present the few nuggets of information available to examine this hypothesis.

Load–life relationships (Norton, 2000) have the general form for uniaxial loading, of

$$N = a \, (\sigma_{ult} / \sigma)^b, \tag{1}$$

or for multiaxial loading,

$$N = a \, (C / P)^b, \tag{2}$$

where N is lifespan (number of loading cycles) and a is a fitting constant. When the load is along a single well defined axis such as simple tension or compression, σ_{ult} is the ultimate breaking or yielding stress (force per cross sectional area) and σ is the stress created by the applied load. For multiaxial loading, C is the ultimate load where failure occurs in a single cycle or causes a transition to rapid failure (i.e. low cycle fatigue, typically manifested as overheating); and P is the applied load. Simultaneous loading along multiple axes creates a critical volume of material rather than a critical cross section, and for that reason stress gradient (N m^{-3}) is emerging as an important parameter in fatigue life studies in both biology (Chaudhry et al., 1997; Tardy et al., 1997; Mulholland et al., 1999) and engineering (Fouvry et al., 1998; Araujo et al., 2004). Notably, for multiaxial fatigue life, the familiar engineering parameter of stress is not an appropriate concept, although engineers typically use an adjustment such as the von Mises method to calculate a uniaxial stress that would create the same distortion energy as the actual combination of applied stresses on multiple axes. The practice of analyzing nearly all mechanical engineering problems in terms of stress is convenient but has perhaps delayed the realization that there are important relationships between force and mass when loading is multiaxial.

The exponent b in the load–life equations is well known for multiaxial loading of certain machine components such as steel ball bearings, where the value is 3 (Norton, 2000). The most thoroughly tested biological material is bone, which in uniaxial tensile or compression shows a b of about 11 (calculated from data in Pattin et al., 1996). Regardless of the material or the precise value of b, reducing the load results in an exponential increase in longevity.

To examine the implications of an exponential increase in lifespan as a function of relative load, it is instructive to consider load–life data for both motor components and whole motors. Steel bearings serve as a good example of a motor component, as they are strong, durable, simple in shape, and

have been tested extensively. Using data from Norton (2000), I calculated the lifespan of steel bearings ranging in mass from 0.06 to 26 kg for loads equal to the critical load C of the smallest bearing (for bearings, C is the load at which lifespan drops below 10^6 cycles; this represents the approximate transition point to rapid breakdown). The resulting curve (Fig. 6) shows how lifespan would increase if load is held constant and bearing mass is increased. Only at loads less than about 1000 N kg^{-1} is lifespan acceptable for devices that rotate at tens or hundreds of cycles per second (i.e. lifetime exceeding tens of millions of cycles). Note that these lifespan estimates are statistical properties of an average bearing; complex motors that depend critically on many bearings would be expected to undergo more rapid failure.

Fig. 6 shows also the only load–life data that I have encountered for a whole motor. These data come from an anonymous reviewer of a draft of Marden and Allen (2002), who stated that: "In practice, a 50 MW gas turbine will weigh 4000 kg as an aircraft engine with a 8000 h life, 16 000 kg when the design is adapted for ground power applications with a 25 000 h life, and 100 000 kg when designed for baseload electric generation with a 100 000 h life." Assuming a specific force output of 57 N kg^{-1} for the aircraft engine and a constant cycle frequency of 390 Hz, the curve in Fig. 6 shows how lifespan increases as the turbine motor is made more massive for applications other than locomotion. The pattern is similar to that for ball bearings, but as expected for a complex structure dependent on many critical parts each subject to stochastic failure (and many parts where loads are concentrated and therefore experience higher specific loads than the motor as a whole), the curve is shifted toward lower specific loads. Fitting a curve to these data predicts a 30% reduction in lifespan at 90 N kg^{-1} and a 40% reduction at 120 N kg^{-1} compared with the lifespan at 57 N kg^{-1}.
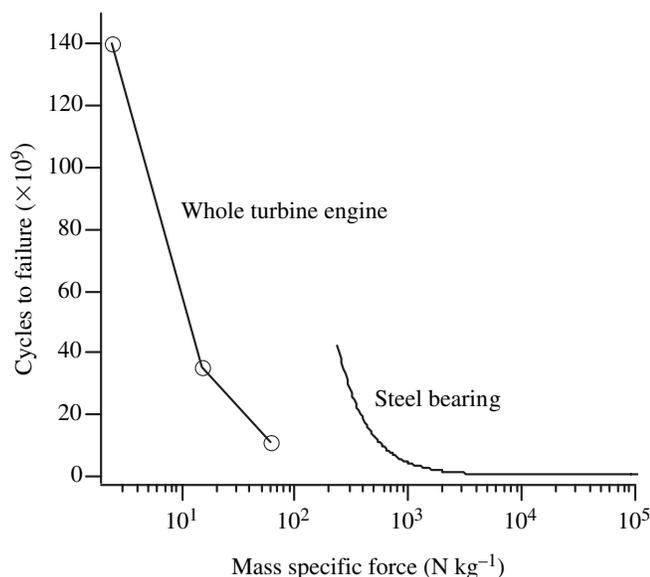
It is possible to perform a similar load–life estimation for a generalized motor based on the data presented in Fig. 2. At 1 kg motor mass, an average translational motor can create a force output of about 890 N. If we assume that this is a critical load (life=1 cycle), this provides the value for C in the load–life equation. Assuming a value of 3 for the exponent b in Equation 2, one can predict the lifespan of a motor with these properties that is cyclically loaded at levels less than 890 N. The resulting prediction (Fig. 7) shows that lifespan is only 209 cycles at 100 N kg^{-1}, but rises to 5600 at 50 N kg^{-1} and 45 000 at 25 N kg^{-1}. Quite obviously there is a large difference in the utility of motors designed to operate over lifespans that would yield only a few dozen *versus* many thousands of cycles and it is the region between 25 and 100 N kg^{-1} where this transition occurs.

The load–life equations (Equations 1, 2) refer to loads that cause high cycle fatigue (HCF). In theory, HCF results from the gradual accumulation of very small damage during each loading cycle until the cumulative damage results in failure (Norton, 2000). What actually occurs in rapidly cycling machinery is somewhat different because shape deformations (residual strain) lead eventually to reductions in recovery of elastic strain energy, increased friction and, ultimately, either breakage or overheating. This type of failure, called low cycle fatigue (LCF), can occur very rapidly once there is a certain level of damage caused by HCF. Therefore, there are transitions from the gradual decrease in lifespan with increased loading due to HCF, to much more rapid transitions due to LCF. There is no equation to model this process, but all
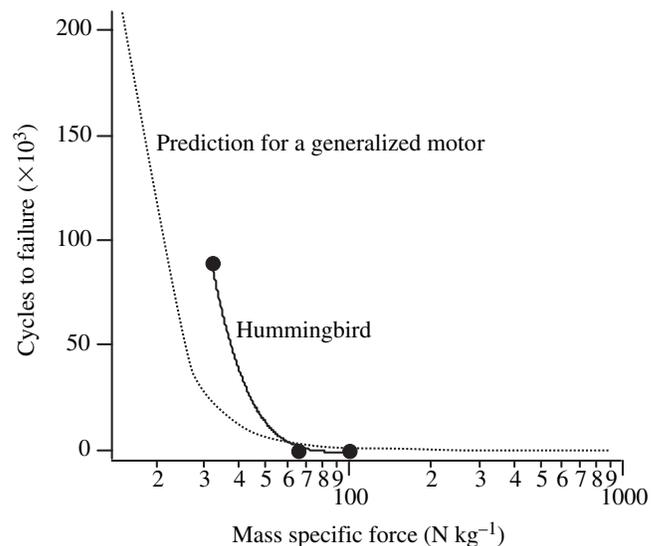

Fig. 7. Predicted lifespan (N cycles) over a range of mass specific force outputs for a generalized 1 kg motor that can withstand a maximal force load of 890 N. This curve assumes that a=1 and b=3 in the load–life equation (Eqn 2). Also shown is a curve relating specific load to the observed number of wingbeat cycles for hummingbirds over one day of normal flight (a highly conservative estimate of cycles to failure) and during experimentally imposed maximal loading.

Fig. 6. Load–life curves for steel bearings (solid circles) and entire turbine engines (open circles).

manufacturers and users of motors understand that certain load levels cause rapid failure.

Despite common knowledge that certain motor loading conditions cause a transition to LCF, it is very difficult to find data showing mass-specific loads at which this occurs. The only such data that I have found come from small electric motors used for model airplane applications (http://www.gws.com.tw/english/product/powersystem/eps-std.htm). These data show how the thrust output of a series of motors (12–133 g) varies across different combinations of propellers, gear ratios, voltage and current. Not surprisingly, maximum specific thrust averages 62 N kg^{-1} (s.d.=12; N=15 motors). The data are limited primarily to sub-maximal thrust and recommended configurations near the maximal thrust. For three of the motors there are also combinations of conditions creating overloads indicated as 'fatally damaging the motor', i.e. low cycle fatigue. A compilation of all of the specific thrust outputs at the different combinations of propeller, gearing, voltage, and current for those three motors shows that LCF tends to occur when specific thrust reaches levels above about 60 N kg^{-1} (dark bars in Fig. 8). The fact that the recommended loads for these motors are very close to their rapid failure point is quite interesting. It suggests that the universal upper limit of specific force output for Group 2 motors is the result of natural and human-imposed selection for motors that can operate close to a transition between high cycle and low cycle fatigue, which appears to occur at specific loads that are generally between 50 and 100 N kg^{-1} (Fig. 9).

Fig. 9. A general model for the load–life curve of motors, with transitions from high-cycle to low-cycle fatigue occurring in the region between about 55–120 N kg^{-1}. In the background is the frequency distribution of specific force output of all Group 2 motors from Fig. 3.

Biological examples of a transition to LCF at a known specific load are scarce, but the work of Chai and Millard (1997) may be applicable. In that study, two species of hummingbirds hovered with maximum muscle mass-specific loads averaging 92–105 N kg^{-1}, but they could maintain that level of performance for less than 0.5 s (about 15 wingbeat cycles). Two smaller hummingbird species lifted specific loads of 64–69 N kg^{-1} for 0.65 s (38–40 wingbeat cycles). At ordinary specific loads (about 33 N kg^{-1} for weight support by a hummingbird whose flight motor is 30% of body mass), hummingbirds fly for many thousands of wingbeat cycles during a single day (10% time in flight during an approximately 8 h day; Schemske, 1975). Including these data for ordinary flight with the data for maximally loaded flight yields the hummingbird load–life curve shown in Fig. 7, which agrees reasonably well with the theoretical curve derived above for motors exposed to cyclical multi-axial stress.

Biological fatigue (e.g. insufficient fuel or oxygen delivery rate) is not necessarily equivalent to structural fatigue. However, it makes sense for biological capacities to evolve so that they match physical constraints, such as the match between hummingbird metabolic rate and their anatomically constrained maximal wing beat amplitude (Chai and Dudley, 1995). Hence, it is reasonable to expect that biological fatigue occurs at conditions close to structural fatigue, which may explain why the rapid failure load for biological motors is very similar to what occurs in engineered motors. This may explain why fruit flies (*Drosophila melanogaster*) that were selected for 160
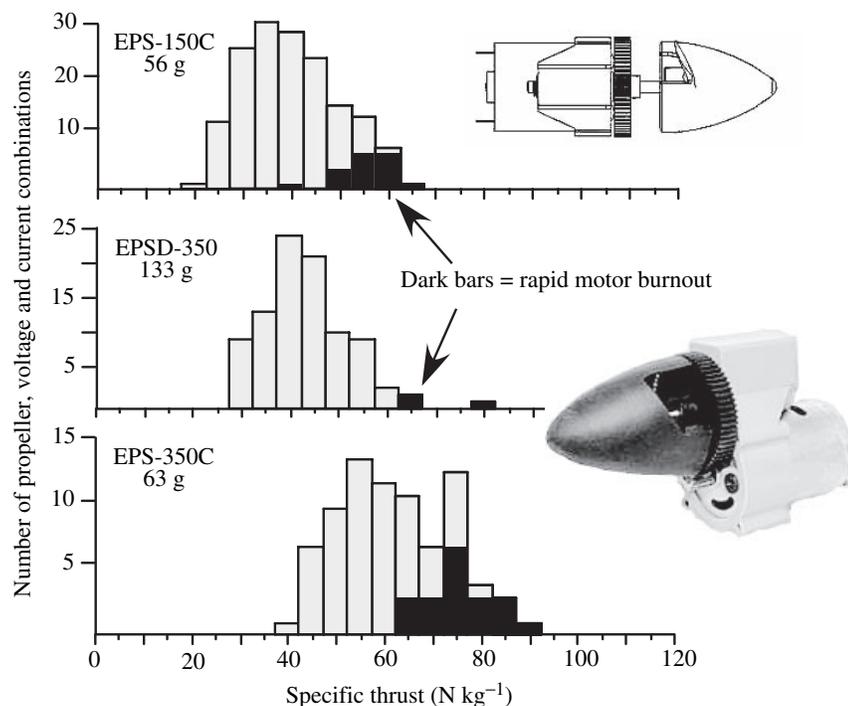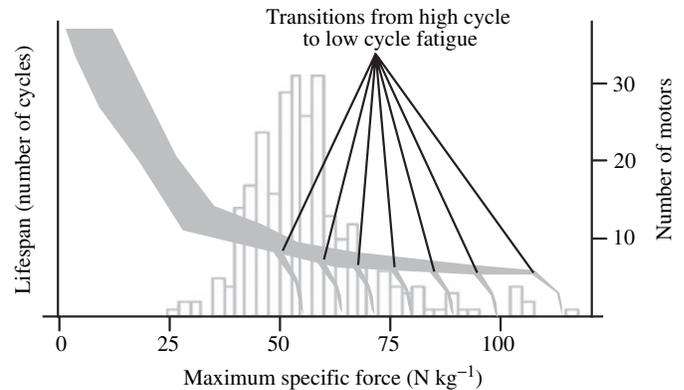

Fig. 8. Specific force output (N kg^{-1} motor mass) for three electric motors used with different combinations of propellers, gear ratios, voltage and current. Dark bars show combinations that are indicated by the manufacturer to cause rapid failure. Superimposed images show a schematic and a photograph of one of these motors, consisting of the motor, gears and propeller nose cone.

generations for ability to fly into an increasingly strong headwind showed a large increase in their mean flight velocity, but showed no increase in maximum velocity (Marden et al., 1997).

Equating muscle with machines in a discussion of structural fatigue may seem questionable due to the self-repair capability of muscle. However, muscle repair occurs on a time scale (hours to days) that is probably not relevant to the time scale over which low cycle fatigue occurs (seconds to minutes). Anyone who has pulled a muscle during peak exertion is unfortunately familiar with the consequences of this difference.

There is also a scaling argument (Table 2) to explain why the force output of all Group 2 motors scales as $M^{1.0}$. Motor force outputs are opposed by the weight and inertia of the devices that they are attached to, as well as the inertia of their own accelerating parts; these forces scale as $M^{1.0}$. Accordingly, relative load (C/P) in the load–life Equation 2 scales as $M^{-0.33}$ for motors in which F_{max} scales as $M^{0.67}$, but is constant (M^0) for motors in which F_{max} scales as $M^{1.0}$. The value of b in the load–life Equation 2 should always be positive (i.e. shorter lifespan at greater loading), which therefore predicts negative scaling of total lifetime cycle number for motors in which relative load (C/P) scales with a mass exponent less than unity, as opposed to a constant number of lifetime cycles for motors having relative loads that scale as $M^{1.0}$. Cycle frequency scales negatively with mass (McMahon and Bonner, 1983) and, therefore, lifespan measured in time rather than cycle number should scale positively, with a mass exponent equal to the mass scaling of cycle period, for motors in which force output scales as $M^{1.0}$. In accord with this hypothesis, animals show a mass-invariant number of total lifetime cycles, positive mass scaling of lifespan (time) and equal mass scaling exponents for cycle period and lifespan (Schmidt-Nielsen, 1984; West et al., 2002).

It should be noted that motors tend to be used most of the time at levels well below their maximum load and, for this reason, behavior has a large impact on motor lifespan. One benefit of having a motor with a high F_{max} is that it provides capability that can be called upon for important transient events. Using a motor near its peak load would sacrifice life in a statistical fashion if used frequently, but certain brief events require high performance (Marden and Chai, 1991) in order to extend lifespan in an absolute fashion (i.e. escaping predators or a human driver entering a busy highway) or to acquire things of great value (i.e. mates; Marden, 1989). The ability to operate for brief periods at specific loads near the transition between HCF and LCF is probably a generally important ability for animals and mobile machines.

How $M^{1.0}$ scaling is achieved mechanistically: a case study using dragonflies

An interesting feature of the fundamental scaling regimes shown in Figs 2 and 3 is that some of the motors in one scaling group are components of motors in the other group. For example, electric motors have force outputs that scale approximately as $M^{1.0}$, yet the force output of whole winches powered by electric motors scales as approximately $M^{0.67}$. A reverse example is that of muscles and animal motors. Individual myosin molecules, muscle cells, and individual muscles have force outputs that scale as $M^{0.67}$, yet they are major components of the animal motor systems whose force outputs scale as $M^{1.0}$. How the scaling of force output changes from components to intact systems has been investigated in running animals (reviewed in Biewener, 2005) and in the dragonfly flight motor (Schilder and Marden, 2004), the latter of which is discussed in detail below.

Like the other motors that show $M^{1.0}$ scaling of force output, the dragonfly flight motor contains levers that affect the magnitude and scaling of force output. The basalar muscle in the dragonfly thorax is connected to the wing in a fashion that is readily understood in terms of the simple lever model for conservation of torque,

$$F_1 D_1 = F_2 D_2, \tag{3}$$

in which F_1 is muscle force output, D_1 is the length of the internal lever arm connecting the basalar muscle to the wing, D_2 is the distance along the wing where the mean aerodynamic force acts, and F_2 is the net aerodynamic force output.

Table 2. *Illustrative example of the scaling of Group 1 and Group 2 motors*

Device mass (kg)	Motor mass (kg)	Motor force output (N)		Relative load (C/P)		Lifetime N cycles		Lifespan (time)	
		Group 1	Group 2	Group 1	Group 2	Group 1	Group 2	Group 1	Group 2
1	0.25	353	15	353	15	44 061 784	3186	59 782 779	4323
10	2.5	1639	147	164	15	4405 976	3186	12 869 335	9307
100	25	7609	1472	76	15	440 577	3186	2770 359	20 035
1000	250	35 318	14 715	35	15	44 056	3186	596 370	43 132
10 000	2500	163 931	147 150	16	15	4405	3186	128 380	92 853
100 000	25 000	760 888	1471 500	8	15	441	3186	27 636	199 892
1000 000	250 000	3531 675	14 715 000	4	15	44	3186	5949	430 323

The scaling of motor force outputs, relative loads (in terms of the ratio of C and P from Equation 2 for the load–life relationship), lifetime number of cycles to failure (using a value of 3 for b in Equation 2), and total lifespan (arbitrary units) for Group 1 motors ($M^{0.67}$ scaling of force output; Fig. 2) and Group 2 motors ($M^{1.0}$ scaling of force output; Fig. 3).

The scaling of the force output of the dragonfly basalar muscle during maximally stimulated isometric tetanus is just as would be expected for a translational motor; it scales as $M^{0.67}$. However, it is important to consider that during locomotion muscles tend to be stimulated by one or a few nerve impulses, their length changes in a cyclical fashion and they produce forces less than maximal isometric tension. Thus, both the magnitude and scaling of force output of muscles during locomotion may be quite different from isometric tetanus. The mean force output of dragonfly basalar muscles during workloop contractions designed to approximate the *in vivo* stress–strain and stimulation regime during maximal flight effort (F_1 in the torque equation for the dragonfly flight motor) scales as $M^{0.83}$. This shift in the scaling exponent is likely due to size-related changes in shortening velocity and duty cycle for muscle activation.

The maximum load that dragonflies can lift scales as $M^{1.03}$ (Marden, 1987; Schilder and Marden, 2004); this provides the scaling of F_2 in the torque equation. The length of the external lever arm (D_2 in the torque equation) is the distance between the wing fulcrum and the second moment of area of the forewing (i.e. the distance at which the mean aerodynamic force acts upon the wing; Ellington, 1984). This distance scales as $M^{0.31}$, very close to the expected scaling slope for geometrically similar dragonflies. The internal lever arm length, D_1, is the distance between the muscle apodeme (a tendon-like connection from the top of the muscle to the wingbase) and the fulcrum of the wing; it scales as $M^{0.54}$, a strong departure from geometrical similarity. It is this combination of the scaling of force output by the working muscle ($M^{0.83}$) and the internal lever arm length ($M^{0.54}$) that explains how the whole-motor force output scales nearly as unity ($M^{1.0}$) for dragonflies that have geometrically similar wing lengths ($M^{0.31}$). [In other words, the sum of the scaling exponents on both sides of the torque equation must be nearly identical (sampling error can make them non-identical for empirical data) and in this example requires F_2 to scale as very nearly $M^{1.0}$].

An interpretation of this result in the context of the preceding discussion of motor lifespan is that the internal lever arm length in dragonflies has evolved in such a fashion that motor performance is maximized while rapid burnout is prevented. As dragonflies evolved away from the size of their common ancestor, they apparently evolved internal lever arm lengths that maintained the $M^{1.0}$ scaling of aerodynamic force output and specific force output in the vicinity of 57 N kg^{-1}. According to the hypotheses presented above, this represents adaptation to three needs – the need for force outputs sufficient to offset body weight and inertia (of both the body and the motor's moving parts), the need to avoid specific loads that exceed a common threshold for LCF, and the need to maintain a sufficiently long motor lifespan. These factors explain why smaller dragonflies have not evolved flight motors that have higher specific force outputs than $M^{0.83}$ scaling of muscle dynamic force would hypothetically allow.

Within all Group 2 motors there must be mechanisms that adjust force output in this fashion, comprising some feature or combination of features in a hierarchal system of linkages that in biological motors might include molecular mechanisms, neural patterns, dynamics of muscle activation, levers and so forth, which together shift the underlying $M^{0.67}$ scaling of muscle tetanic force to $M^{1.0}$ scaling of whole-motor force output in the neighborhood of 57 N kg^{-1} during rapid cyclical contraction.

Rockets considered separately

Rockets do not push or pull against a fixed load or generate a critical stress related to their cross sectional area as do other Group 1 motors. Why then does the force output of rockets also scale as $M^{0.67}$? The answer is that the thrust produced by a rocket is determined by the mass flow rate, which depends on the cross sectional area of the throat and nozzle from which gas is ejected (http://www.grc.nasa.gov/WWW/K-12/airplane/rockth.html presents an explanation of the basic physics). Area dependence of mass flow rate means that the maximum thrust of rockets should scale as $M^{0.67}$ just as it does in other types of translational motors. Furthermore, rockets are used only once, or at most a few times, and have burn times measured in seconds or minutes. Their F_{max} is therefore not subject to fatigue or life span constraints.
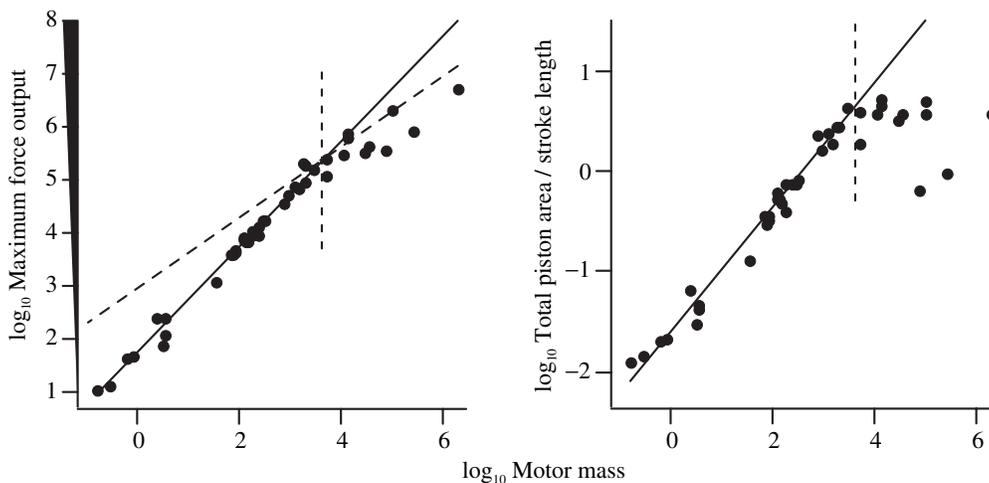

Fig. 10. Scaling of maximum force output (A) and ratio of total piston cross sectional area to stroke length (B) in relation to motor mass over the entire size range of piston engines. The vertical dashed line indicates the crossing point of the scaling fits for Group 1 (dashed line) and Group 2 (solid line) motors. Maximum force output (N), motor mass (kg), total piston area/stroke length (m^2 $^{-1}$).

Maximum specific thrust of rockets is actually higher than the values that we report because we use takeoff mass, which includes all of the fuel. Thrust as a function of mass during the course of a rocket burn can be complex, but for present purposes it is sufficient to note that high values of thrust can be generated when there is much less than a full load of fuel, particularly for liquid fuel rockets that pump the fuel to the ignition chamber. For this reason, the thrust values for rockets in the data plotted here are conservative.

$M^{0.67}$ scaling has some interesting consequences for applications of rockets. At the lower end of the size range, $M^{0.67}$ scaling creates very high thrust-to-weight ratios (i.e. acceleration) that allow small missiles to easily overtake jet powered aircraft. This would not be possible for missiles powered by anything other than small rocket engines, which are the only motors that produce both exceptionally high specific thrust and high speed. As mass increases, the specific thrust at takeoff declines steadily to values as low as 15–25 N kg^{-1} for the first stage of the Saturn and Titan rockets and the solid rocket boosters of the Space Shuttle. At least 9.8 N kg^{-1} is needed to lift off from the ground, which is why the payload is so small in comparison to the motor size in these applications. These rockets use enormous size rather than high specific performance to accomplish the job, and there seems to be little potential for the size of rockets useable for flight to increase substantially beyond these extant designs.

Really big motors: what happens when major scaling regimes collide

An interesting feature of the two distinct scaling relationships shown in Figs 2 and 3 is that they intersect at a mass of approximately 4400 kg. If the force output of Group 2 motors were to continue to scale as $M^{1.0}$ at motor masses greater than 4400 kg, they would need to produce more force per cross sectional area than do Group 1 motors. This seems unlikely, since the force output of Group 1 motors appears to be limited by critical stress across their cross sectional area. An axial stress strong enough to break a Group 1 motor should also break a Group 2 motor. Therefore, the scaling of force production by Group 2 motors should change from $M^{1.0}$ to $M^{0.67}$ at motor masses greater than 4400 kg.

Marden and Allen (2002) tested this prediction by examining data (Fig. 10) for piston engines ranging in size from 0.17 to 1,901,000 kg (model airplanes to oil tankers; Fig. 11 shows a cross section of one such very large motor). The $M^{1.0}$ scaling equation for all other Group 2 motors fits precisely the sample of piston engines less than 4400 kg, whereas the $M^{0.67}$ scaling equation for Group 1 motors fits the upper bound of force output for piston engines greater than 4400 kg. Analysis of covariance shows that separate regression lines fit to these data for motors above and below 4,400 kg have significantly different slopes ($P<0.0001$). The inflection point at 4400 kg is even more pronounced for geometric data (Fig. 10). A tight relationship that describes the mass scaling
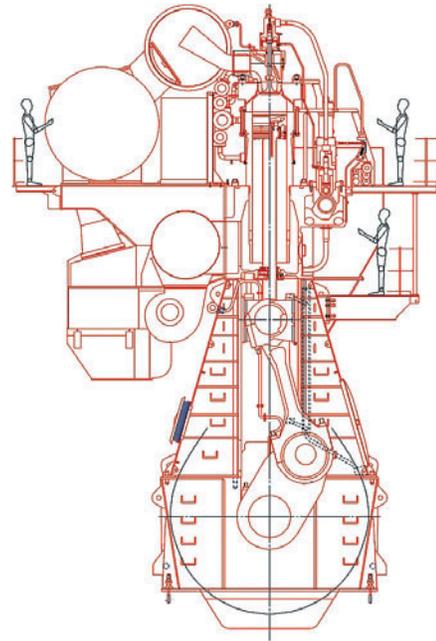

Fig. 11. Cross sectional schematic of one of the largest piston engine (Burmeister and Wain K98MC-C) and three of its human operators. The geometry of piston engines larger than 4400 kg departs radically from what would be predicted from the scaling of smaller piston engines; this departure begins at the crossing point of the scaling relationships for Group 1 and Group 2 motors. Reproduced with permission from B&W Engine Selection Guide, February 2000.

of the ratio of total piston cross-sectional area to stroke length (chosen because this index captures two geometric variables) across four orders of magnitude up to a mass of 4400 kg does not apply for larger engines, which show a great diversification in their design.

As a result of the shift from $M^{1.0}$ to $M^{0.67}$ scaling of piston engine force output in motors greater than 4400 kg, the specific force of the largest piston engines is dramatically reduced. The largest piston engine, the Burmeister & Wain K98MC-C (Fig. 11; mass=1.9×10^6 kg), used to propel oil tankers produces a specific force output of only 3 N kg^{-1}. An important consequence of such low specific force output is that it contributes (along with large payload) to the very slow acceleration and deceleration ability of oil tankers and increases their risk of collision with other ships and obstacles. The pilot of an oil tanker must react to obstacles with a tremendous amount of forethought because the inertia of the vessel cannot be counteracted over a short time or distance.

List of symbols

M	mass of a motor (kg)
F_{max}	maximum force output (N) by a motor
HCF	high cycle fatigue
LCF	low cycle fatigue
L	length
N	total number of cycles prior to failure, yield, or low cycle fatigue
N	force (Newtons)
σ_{ult}	ultimate stress (N m^{-2}) prior to failure or yield
σ	applied stress (N m^{-2})
C	ultimate load (N) prior to failure, yield, or low cycle fatigue
P	applied load (N)
b	exponent relating relative load to fatigue lifespan
F_1	force output (N) by a muscle
F_2	force output (N) by a wing
D_1	distance (m) between a muscle and wing fulcrum
D_2	distance (m) between a wing fulcrum and the wing second moment of area

References

Alexander, R. M. (1985). The maximum forces exerted by animals. *J. Exp. Biol.* **115**, 231-238.

Araujo, J. A., Nowell, D. and Vivacqua, R. C. (2004). The use of multiaxial fatigue models to predict fretting fatigue life of components subjected to different contact stress fields. *Fatigue Fracture Engin. Mat. Struct.* **27**, 967-978.

Barragan, A. and Sibley, L. D. (2003). Migration of Toxoplasma gondii across biological barriers. *Trends Microbiol.* **11**, 426-430.

Biewener, A. A. (2005). Biomechanical consequences of scaling. *J. Exp. Biol.* **208**, 1665-1676.

Blob, R. W. and Biewener, A. A. (2001). Mechanics of limb bone loading during terrestrial locomotion in the green iguana (*Iguana iguana*) and American alligator (*Alligator mississippiensis*). *J. Exp. Biol.* **204**, 1099-1122.

Bowlin, M. S. and Winkler, D. W. (2004). Natural variation in flight performance is related to timing of breeding in the tree swallow *Tachycineta bicolor*. *The Auk* **121**, 345-353.

Chai, P. and Dudley, R. (1995). Limits to vertebrate locomoter energetics suggested by hummingbirds hovering in heliox. *Nature* **377**, 722-725.

Chai, P. and Millard, D. (1997). Flight and size constraints: hovering performance of large hummingbirds under maximal loading. *J. Exp. Biol.* **200**, 2757-2763.

Chaudhry, H. R., Bukiet, B., Davis, A., Ritter, A. B. and Findley, T. (1997). Residual stresses in oscillating thoracic arteries reduce circumferential stresses and stress gradients. *J. Biomech.* **30**, 57-62.

Dickinson, M. H., Lehmann, F. O. and Sane, S. P. (1999). Wing rotation and the aerodynamic basis of insect flight. *Science* **284**, 1954-1960.

Dillon, M. E. and Dudley, R. (2004). Allometry of maximum vertical force production during hovering flight of neotropical orchid bees (Apidae: Euglossini). *J. Exp. Biol.* **207**, 417-425.

Dobrowolski, J. M. and Sibley, L. D. (1996). Toxoplasma invasion of mammalian cells is powered by the actin cytoskeleton of the parasite. *Cell* **84**, 933-939.

Dudley, R. (2002). *The Biomechanics of Insect Flight: Form, Function, Evolution.* Princeton, N.J.: Princeton University Press.

Ellington, C. P. (1984). The aerodynamics of hovering insect flight. II. Morphological parameters. *Phil. Trans. R. Soc. Lond. B* **305**, 17-40.

Ellington, C. P. (1999). The novel aerodynamics of insect flight: applications to micro-air vehicles. *J. Exp. Biol.* **202**, 3439-3448.

Epstein, A. H., Jacobson, S. A., Protz, J. M. and Frechette, L. G. (2000). Shirtbutton-sized gas turbines: the engineering challenges of micro high speed rotating machinery. In *8th International Symposium on Transport Phenomena and Dynamics of Rotating Machinery*. Honolulu, HI.

Epstein, A. H. and Senturia, S. D. (1997). Microengineering: macro power from micro machinery. *Science* **276**, 1211.

Finer, J. T., Simmons, R. M. and Spudich, J. A. (1994). Single myosin molecule mechanics: piconewton forces and nanometre steps. *Nature* **368**, 113-119.

Fischer, P., Dannbauer, H. and Unger, B. (1998). Fatigue analysis to accelerate design process of a Diesel engine. In *CIMAC (22nd International Congress on Combustion Engines)*, pp. 11. Copenhagen.

Fouvry, S., Kapsa, P., Sidoroff, F. and Vincent, L. (1998) Identification of the characteristic length scale for fatigue cracking in fretting contacts. *J. Physique* IV 8 (P8), 159-166.

Full, R., Yamauchi, A. and Jindrich, D. (1995). Maximum single leg force production: cockroaches righting on photoelastic gelatin. *J. Exp. Biol.* **198**, 2441-2452.

Iriarte-Diaz, J. (2002). Differential scaling of locomotor performance in small and large terrestrial mammals. *J. Exp. Biol.* **205**, 2897-2908.

Marden, J. H. (1987). Maximum lift production during takeoff in flying animals. *J. Exp. Biol.* **130**, 235-258.

Marden, J. H. (1989). Bodybuilding dragonflies: costs and benefits of maximizing flight muscle. *Physiol. Zool.* **62**, 505-521.

Marden, J. H. and Allen, L. R. (2002). Molecules, muscles and machines: universal performance characteristics of motors. *Proc. Natl. Acad. Sci. USA* **99**, 4161-4166.

Marden, J. H. and Chai, P. (1991). Aerial predation and butterfly design: how palatability, mimicry and the need for evasive flight constrain mass allocation. *Am. Nat.* **138**, 15-36.

Marden, J. H., Wolf, M. R. and Weber, K. E. (1997). Aerial performance of *Drosophila melanogaster* from populations selected for upwind flight ability. *J. Exp. Biol.* **200**, 2747-2755.

Mattheck, C. (1998). *Design in Nature: Learning from Trees*. Heidelberg: Springer Verlag.

Mattingly, J. D. (2002). *Aircraft Engine Design*. Reston, VA: American Institute of Aeronautics and Astronautics.

McHenry, M. J. and Jed, J. (2003). The ontogenetic scaling of hydrodynamics and swimming performance in jellyfish (*Aurelia aurita*). *J. Exp. Biol.* **206**, 4125-4137.

McMahon, T. A. and Bonner, J. T. (1983). *On Size and Life*. New York: Scientific American.

Mulholland, S. E., Lee, S., McAuliffe, D. J. and Doukas, A. G. (1999). Cell loading with laser-generated stress waves: the role of the stress gradient. *Pharm. Res.* **16**, 514-518.

Niebur, G. L., Feldstein, M. J. and Keaveny, T. M. (2002). Biaxial failure behavior of bovine tibial trabecular bone. *J. Biomech. Eng.* **124**, 699-705.

Norton, R. L. (2000). *Machine Design: An Integrated Approach*. Upper Saddle River, N.J.: Prentice Hall.

Orchard, J. W., Alcott, E., James, T., Farhart, P., Portus, M. and Waugh, S. R. (2002). Exact moment of a gastrocnemius muscle strain captured on video. *Br. J. Sports Med.* **36**, 222-223.

Pattin, C. A., Caler, W. E. and Carter, D. R. (1996). Cyclic mechanical property degradation during fatigue loading of cortical bone. *J. Biomech.* **29**, 69-79.

Schemske, D. W. (1975). Time budget and foraging site preference of the Cinnamon Hummingbird in Costa Rica. *Condor* **77**, 216-217.

Schilder, R. J. and Marden, J. H. (2004). A hierarchical analysis of the scaling of force production by dragonfly flight motors. *J. Exp. Biol.* **207**, 767-776.

Schmidt-Nielsen, K. (1984). *Scaling: Why is Animal Size so Important?* Cambridge: Cambridge University Press.

Sibley, L. D. (2004). Intracellular parasite invasion strategies. *Science* **304**, 248-253.

Sonsino, C. M. (2001). Influence of load and deformation-controlled multiaxial tests on fatigue life to crack initiation. *Int. J. Fatigue* **23**, 159-167.

Tardy, Y., Resnick, N., Nagel, T., Gimbrone, M. A., Jr and Dewey, C. F., Jr (1997). Shear stress gradients remodel endothelial monolayers in vitro via a cell proliferation-migration-loss cycle. *Arterioscler. Thromb. Vasc. Biol.* **17**, 3102-3106.

Vogel, S. (1988). Life's Devices. Princeton, N.J.: Princeton University Press.

West, G. B., Woodruff, W. H. and Brown, J. H. (2002). Allometric scaling of metabolic rate from molecules and mitochondria to cells and mammals. *Proc. Natl. Acad. Sci. USA* **99 (Suppl. 1)**, 2473-2478.

Wickman, P. O. (1992). Sexual selection and butterfly design – a comparative study. *Evolution* **46**, 1525-1566.